Regularization Techniques for Floor Plan Estimation in Radio Tomographic Imaging

Brian Beck, Robert Baxley
Communications, Systems, and Spectrum Division
Georgia Tech Research Institute
Atlanta GA, USA 30318
email: bbeck6@gatech.edu, bob.baxley@gtri.gatech.edu

Xiaoli Ma
Georgia Institute of Technology
Atlanta GA, USA 30318
email: xiaoli@gatech.edu

***Abstract*—An important potential application of Radio Tomographic Imaging is the estimation of building floor plans and interior features in a wireless network. This paper proposes a novel technique for the regularization of solutions to RTI problems with the goal of enhancing building floor plan images. This is done by exploiting *a-priori* information about the structure, and therefore spatial covariance, of typical buildings. An elliptically-shaped covariance function is used to better model the spatial covariances of pixels in floor plan images. Our approach is verified through simulation, showing improvements over the widely applied Tikhonov regularization method. Our results show reductions in mean-squared error, while also increasing SSIM, a popular measure of subjective image quality.**

I. Introduction

Radio Tomographic Imaging (RTI) is a technique for imaging objects which are shadowing the links in a wireless sensor network. Each node in the sensor network takes measurements of the received signal strength (RSS) from all other nodes. By compiling the measurement data together and using an appropriate forward/inverse model, an estimate of the area's shadowing, or spatial loss field (SLF) can be formed. This estimated image represents the amount of RF attenuation in dB that is seen at each pixel location. An RTI system could be used to track objects or people that are located within a wireless network [1], [2]. Another important application of RTI is the imaging of static objects such as building floor plans [3], [4]. RTI can provide information about the layout of a building, even interior walls and features otherwise obstructed from line-of-sight viewing. A tomographic estimate of the building's interior layout can be generated using wireless links placed outside the building, since the interior may not be accessible. This paper focuses on this static floor plan imaging problem.

One of the important challenges in RTI is the ill-conditioned nature of the inverse problem. Because there are a limited number of links in the network, there is generally insufficient data to form a unique image of the environment. To deal with this challenge, a regularization method is needed. Regularization is a process of applying additional model constraints to enforce a unique solution, while still agreeing with the data as much as possible [5]. Tikhonov regularization is one of the most common techniques. It was favored in [6] and [7] for being a reasonable compromise between computational complexity and quality of image reconstruction in RTI. In this paper we will use the Tikhonov approach as the basis for comparison with our proposed method.

In this paper we propose a novel technique for regularizing RTI problems in which the subject is a building floor plan. Our approach involves applying a unique elliptical shape to the spatial covariance function, which defines the *a-priori* covariances that exist between image pixels. This is in line with the Bayesian approach to regularization, which is outlined in Section III. Further, we observe that the SLF image must be non-negative, which we apply as a constraint to the regularization. Our example reconstructions and comprehensive simulation results show significant improvements to objective image estimate accuracy, as well as to subjective image quality.

II. RTI Linear Model

RTI employs a linear forward model to map an unknown spatial loss field (SLF) to a set of RSS measurements at multiple receiver/transmitter locations. The model of [1] is summarized here. The SLF represents the RF attenuation in dB that occurs at a given pixel location, and indicates the presence of solid objects. Each node in the network measures the RSS from all other nodes. For K nodes in the network, and an SLF image $\mathbf{g} \in \mathbb{R}^{MN\times 1}$, the linear model is given by

$$\boldsymbol{\eta} = \mathbf{B}\mathbf{g} + \mathbf{n}\,, \tag{1}$$

where $\boldsymbol{\eta} \in \mathbb{R}^{K(K-1)\times 1}$ is a vector of RSS measurements, $\mathbf{B} \in \mathbb{R}^{K(K-1)\times MN}$ is a *known* weighting matrix, and $\mathbf{n}$ is a vector of white Gaussian noise. Elements of the $\mathbf{B}$ matrix are assigned by an ellipse between each pair of nodes in the network, with the nodes as foci. If the center of a pixel resides inside the ellipse, then it is assigned weight $1/\sqrt{d}$, with d as the distance between the nodes.

III. Tikhonov and Bayesian Regularizations

In this section we show the close relationship between the Tikhonov and Bayesian approaches to regularization. Our method borrows elements from each. Without regularization, a pure least-squares solution is unusable since the operator $\mathbf{B}$ is underdetermined. To correct this, the Tikhonov approach adds an additional norm constraint on the unknown image:

$$\hat{\mathbf{g}} = \arg\min_{\mathbf{g}} \|\mathbf{B}\mathbf{g} - \boldsymbol{\eta}\|_2^2 + \alpha\|\boldsymbol{\Gamma}\mathbf{g}\|_2^2\,, \tag{2}$$

where $\alpha > 0$ is a scalar weight parameter and $\mathbf{\Gamma} \in \mathbb{R}^{MN \times MN}$ is a known matrix [8]. In [1], $\mathbf{\Gamma}$ represents a first derivative operator, thus enforcing a smoothness constraint on $\mathbf{g}$. The parameter α controls the amount of regularization to apply; larger values of α will promote smoother images. The closed-form solution to (2) is given by

$$\hat{\mathbf{g}} = \left(\mathbf{B}^T\mathbf{B} + \alpha\mathbf{\Gamma}^T\mathbf{\Gamma}\right)^{-1}\mathbf{B}^T\boldsymbol{\eta}\,. \tag{3}$$

Alternatively, one may take a Bayesian approach to regularization. In the Bayesian view, the image $\mathbf{g}$ is viewed as a random variable, and thus has a probability distribution given the observations, i.e., $p(\mathbf{g}|\boldsymbol{\eta}) \propto p(\boldsymbol{\eta}|\mathbf{g})\,p(\mathbf{g})$. Here *a-priori* information about the image $\mathbf{g}$ is used, in the form of the prior probability distribution on the image, $p(\mathbf{g})$. The properties of this distribution may be chosen to represent beliefs about the unknown image in the absence of data. After defining the posterior distribution, taking its expected value $E\left[p(\mathbf{g}|\boldsymbol{\eta})\right]$ results in an MMSE estimate of $\mathbf{g}$. For example, in the Gaussian linear model of (1), if it is assumed that $p(\mathbf{g}) \sim N(\mathbf{0}, \mathbf{C}_g)$, then this MMSE estimate is given by (cf. [9])

$$\hat{\mathbf{g}}_{MMSE} = \left(\mathbf{B}^T\mathbf{B} + \mathbf{C}_g^{-1}\right)^{-1}\mathbf{B}^T\boldsymbol{\eta}\,, \tag{4}$$

under the additional assumption that the data are uncorrelated. We can immediately see the close relationship between the solutions (3) and (4). The matrices $\mathbf{\Gamma}$ and $\mathbf{C}_g^{-1}$ are related via the Cholesky decomposition, thus allowing one to be solved for in place of the other. $\mathbf{C}_g$ represents our *a-priori* assumptions about the *spatial covariances* of pixels in the image. The Bayesian approach is useful here because one may have significant prior knowledge of general image structure, as in the case of building floor plans. Our approach is not equivalent to (4), because we will not assume $p(\mathbf{g})$ is Gaussian, but we will still define and use a covariance matrix as in the Bayesian case. Also, our method will minimize a cost function very similar to (2), much like the Tikhonov approach.

IV. Elliptical Spatial Covariance Regularization

In this section we outline our proposed approach for improved regularization of floor plan images. One way to define the matrix $\mathbf{C}_g$ is to assume an *a-priori* pixel variance σ_g^2, which then decays exponentially with distance:

$$[\mathbf{C}_g]_{i,j} = \sigma_g^2\, e^{-\frac{d_{ij}}{\kappa}}\,, \tag{5}$$

where d_{ij} is the distance between pixels i and j, and κ is a spread parameter controlling how quickly the covariance decays with distance. This function has been used in [10], [11] to model link shadow fading in wireless networks, and noted in [1] for approximating the covariances resulting from the random placement of objects in space. This causes the pixel covariance to fall off equally in all directions, which might be appropriate when no information about the image structure is available.

We propose to extend this function to incorporate further prior information about building features. In the floor plan imaging scenario, certain building features are highly recurrent. First, structural parts of a building tend to be made from homogeneous materials, thus giving large portions of the floor plan a constant RF attenuation value. Second, most floor plan structures, such as interior/exterior walls, are either parallel or orthogonal to each other, with length much greater than width. We can capture a significant amount of this knowledge by extending the covariance function (5) to an elliptical shape with tunable parameters:

$$[\mathbf{C}_g]_{i,j} = \sigma_g^2\, \exp\left[-\sqrt{\left(\frac{d_{x,ij}}{\kappa_x}\right)^2 + \left(\frac{d_{y,ij}}{\kappa_y}\right)^2}\right]. \tag{6}$$

Here, $d_{x,ij}$ and $d_{y,ij}$ represent the distance between pixels i and j in the x and y directions, respectively. The spread parameters κ_x, κ_y control the rate at which the function falls off in the x and y directions independently. By adjusting κ_x and κ_y, the shape of the ellipse can be controlled. Thus by setting $\kappa_x >> \kappa_y$, the spatial covariance becomes highly oriented in the x direction. An example covariance function for a single pixel is plotted in Fig.1. Defining the spatial covariance in this way will emphasize pixels close to pixel $(16, 16)$, but in the x direction only, e.g., if the given pixel is part of a wall.

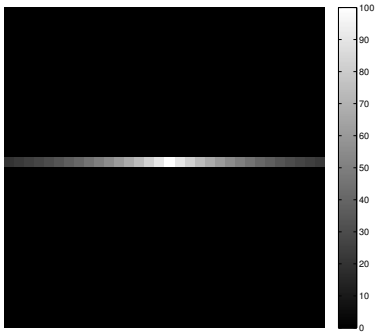

Fig. 1. Elliptical covariance function for pixel (16,16) in a 32×32 pixel image. Here $\kappa_x = 10$ (m), $\kappa_y = 0.2$ (m). The assumed pixel variance is $\sigma_x^2 = 100$ (dB^2).

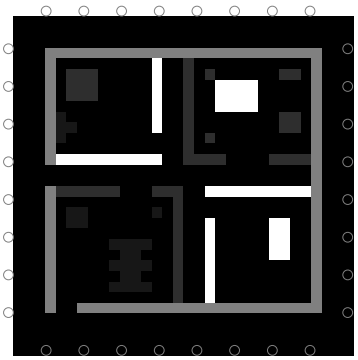

Fig. 2. Original 32×32 pixel SLF image used in the example and training of parameters. The number of nodes, $K = 32$ (gray circles); the area measures 32×32 meters. A white pixel represents 30dB of RF attenuation.

For the case of walls or other floor plan features that are orthogonal to those given in Fig.1, we employ a rotation of the function (6), by transforming the distance values $d_{x,ij}$, $d_{y,ij}$. This transformation is given by

$$\begin{bmatrix} d^{\perp}_{x,ij} \\ d^{\perp}_{y,ij} \end{bmatrix} = \begin{bmatrix} \cos\theta & -\sin\theta \\ \sin\theta & \cos\theta \end{bmatrix} \begin{bmatrix} d_{x,ij} \\ d_{y,ij} \end{bmatrix}, \tag{7}$$

where the angle $\theta = 90$ degrees. Thus, from (6) and (7) there are *two* covariance matrices, one emphasizing image features in the horizontal direction, and the other in the vertical direction. We denote these matrices as $\mathbf{C}_g$ and $\mathbf{C}_g^{\perp}$, respectively. This will produce two separate image estimates, one for each direction. These estimates are found by minimizing the functions

$$\begin{aligned} \hat{\mathbf{g}} &= \arg\min_{\mathbf{g}>0} \|\mathbf{B}\mathbf{g} - \boldsymbol{\eta}\|_2^2 + \mathbf{g}^T \mathbf{C}_g^{-1} \mathbf{g} \\ \hat{\mathbf{g}}^{\perp} &= \arg\min_{\mathbf{g}>0} \|\mathbf{B}\mathbf{g} - \boldsymbol{\eta}\|_2^2 + \mathbf{g}^T \mathbf{C}_g^{\perp -1} \mathbf{g}\,. \end{aligned} \tag{8}$$

Note that the functions in (8) are rearrangements of the Tikhonov regularization (2) to accommodate the $\mathbf{C}_g$ matrices directly. We have also added the constraint that each element of $\mathbf{g}$ must be greater than zero. This is due to the observation that a spatial loss field must be positive or zero everywhere. While the functions in (8) do not have closed form solutions, they are convex, and can be solved using efficient algorithms. For this paper we have employed the CVX package [12] to find the optimal estimates $\hat{\mathbf{g}}$ and $\hat{\mathbf{g}}^{\perp}$. We have also assumed that the building's orientation with respect to the x axis is known by observing the exterior of the structure. However, our results could be easily extended to an unknown orientation by rotating the coordinate system and performing multiple image reconstructions, keeping the solution which minimizes (8).

While the image estimates could be viewed separately, it is desirable to have only a single representation of the scene. To accomplish this, a method of fusing the component images must be chosen. While the images could simply be averaged together, methods exist from the image processing literature that seek to preserve the most perceptible features from the component images, while rejecting others. In our case, we seek to reconstruct images which tend to consist of straight, piecewise constant sections. Additionally, the covariance matrix $\mathbf{C}_g$ will tend to blur its image estimate in the x direction, and $\mathbf{C}_g^{\perp}$ will blur its estimate in the y direction. For these reasons, we have selected the method of contrast pyramids introduced in [13], [14]. This method acts to strongly preserve edge information in both component images, while acting to filter out the directional blurring that has occurred. The Image Fusion Toolbox code by Rockinger [15] was used to merge the images.

To demonstrate the performance of our proposed approach, we have performed tomographic reconstructions on the example SLF image of Fig.2. The reconstruction of Fig.3 was performed using the standard first-difference Tikhonov regularization of equation (2), with the parameter α optimized using the L-curve method. That is, α is chosen corresponding to the point of maximum curvature on a plot of $\|\boldsymbol{\Gamma}\mathbf{g}\|_2$ vs $\|\mathbf{B}\mathbf{g} - \boldsymbol{\eta}\|_2$. In Fig.4, we have used our proposed elliptical covariance approach for the reconstruction. The regularization parameters were determined using a grid search over possible values, and the set minimizing the MSE $\|\hat{\mathbf{g}} - \mathbf{g}\|_2^2$ were chosen. We note from the example results that our method has the potential to significantly lower the image MSE, improve edge contrast, and raise overall subjective image quality.

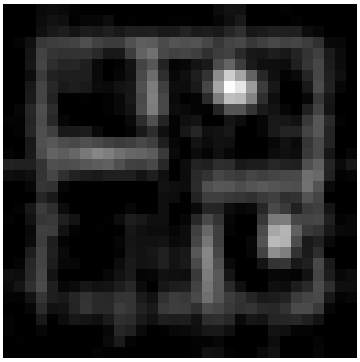

Fig. 3. Reconstruction of the image of Fig.2, using Tikhonov regularization. The regularization parameter $\alpha = 1.0$, found using the L-curve method. Image MSE $= 30.5$, SSIM $= 0.735$.

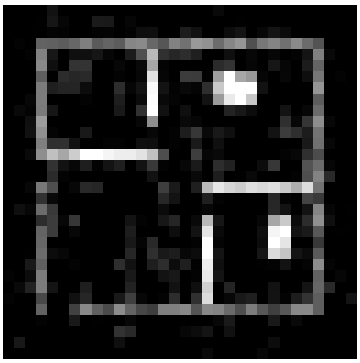

Fig. 4. Reconstruction of the image of Fig.2, using our proposed method. The regularization parameters $\sigma_g^2 = 100$, $\kappa_x = 10$, and $\kappa_y = 0.2$. Image MSE $= 8.07$, SSIM $= 0.931$.

V. Comprehensive Simulation

Two comprehensive simulations were performed to measure the quality of our model relative to the standard Tikhonov regularization. To measure performance, we use the traditional mean squared error criterion for objective image estimate accuracy. To measure the subjective image quality improvements, we employ the widely used SSIM image quality metric [16]. This metric attempts to measure structure within an image, which the human observer is sensitive to. For this metric, higher values are better, with SSIM $= 1$ indicating that two images are identical.

For the simulations, 200 random floor plan images were generated for each data point. Each random image consists of two to eight wall sections in each of the horizontal and vertical directions, with each wall section having random length and random RF attenuation in the range [3 30] dB. MSE and SSIM

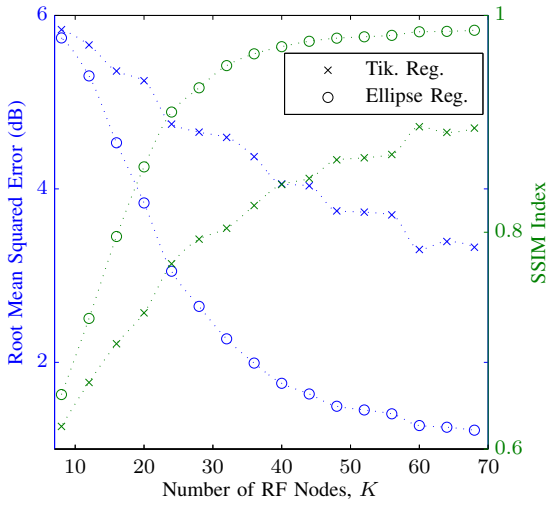

Fig. 5. First comprehensive simulation results, 200 random images per data point. The measurement noise $\sigma_\eta^2 = 9$.

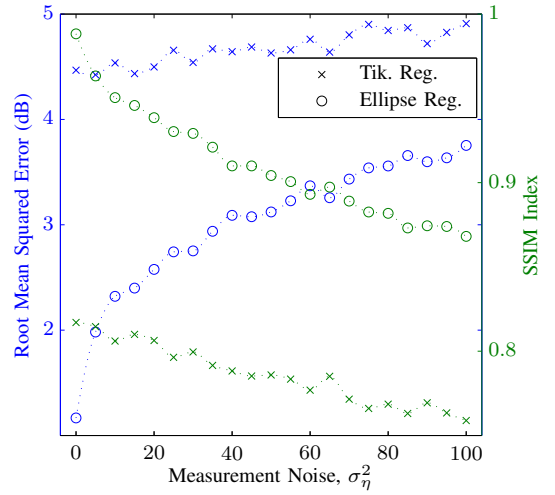

Fig. 6. Second comprehensive simulation results, 200 random images per data point. The number of nodes $K = 32$.

values are averaged to obtain each data point. The L-curve method is used for all Tikhonov reconstructions independently, i.e., a new optimal α value is computed for *each* random image. For our elliptical covariance approach, we have used the same set of regularization parameters found in Section IV for *all* reconstructions, thus leaving them constant.

In the first simulation, the number of RF nodes is varied, with measurement noise held constant at $\sigma_\eta^2 = 9$. The results are plotted in Fig.5. From this we can see both a significant drop in average MSE, as well as improvement to the subjective SSIM metric over a large number of RF nodes. In the second simulation, plotted in Fig.6, the number of RF nodes is constant at $K = 32$, and the measurement noise is varied. We again observe lower MSE, and higher SSIM values for our proposed approach over a wide range of noise levels. We note the consistent improvement of our method over a large number of scenarios, indicating robustness of our model to the choice of regularization parameters.

VI. Conclusions and Future Work

In this paper we have introduced a novel method for improving the regularization of floor plan image reconstructions in RTI. The examples and comprehensive simulation results show its potential for use in obtaining more accurate images from given measurement data. Results also indicate that the method is robust to the choice of regularization parameters. Future research could focus on actively determining the regularization parameters without initial training, as well as removing prior knowledge of the building's orientation. Our work could also be applied to other tomography problems in which thin, piecewise constant image sections are prevalent.

References

[1] J. Wilson and N. Patwari, "Radio tomographic imaging with wireless networks," *Mobile Computing, IEEE Transactions on*, vol. 9, pp. 621–632, 2010.

[2] ——, "See-through walls: Motion tracking using variance-based radio tomography networks," *Mobile Computing, IEEE Transactions on*, vol. 10, no. 5, pp. 612–621, May 2011.

[3] B. Beck, R. Baxley, and X. Ma, "Improving radio tomographic images using multipath signals," in *Proc. Wireless Information Technology and Systems, IEEE International Conference on (ICWITS)*, 2012, pp. 1–4.

[4] B. R. Hamilton, X. Ma, R. Baxley, and S. M. Matechik, "Radio frequency tomography in mobile networks," in *Proc. IEEE Statistical Signal Processing Workshop*, Aug. 2012, pp. 508–511.

[5] P. Hansen, *Rank-Deficient and Discrete Ill-Posed Problems: Numerical Aspects of Linear Inversion*, ser. Monographs on Mathematical Modeling and Computation. Society for Industrial and Applied Mathematics, 1987.

[6] J. Wilson, N. Patwari, and F. Vasquez, "Regularization methods for radio tomographic imaging," in *Proc. Wireless Personal Communications, Virginia Tech Symposium on*, 2009.

[7] H. Liu, Z. Wang, X. Bu, and J. An, "Image reconstruction algorithms for radio tomographic imaging," in *Proc. Cyber Technology in Automation, Control, and Intelligent Systems, IEEE International Conference on (CYBER)*, 2012.

[8] R. Aster, B. Borchers, and C. Thurber, *Parameter Estimation and Inverse Problems*, 2nd ed. Academic Press, 2012.

[9] A. M. Stuart, "Inverse problems: A bayesian perspective," *Acta Numerica*, vol. 19, pp. 451–559, Apr. 2010.

[10] N. Patwari and P. Agrawal, "NESH: A joint shadowing model for links in a multi-hop network," in *Proc. Acoustics, Speech and Signal Processing, IEEE International Conference on (ICASSP)*, Apr. 2008, pp. 2873–2876.

[11] P. Agrawal and N. Patwari, "Correlated link shadow fading in multi-hop wireless networks," *Wireless Communications, IEEE Transactions on*, vol. 8, no. 8, pp. 4024–4036, 2009.

[12] M. Grant and S. Boyd, "Graph implementations for nonsmooth convex programs," in *Recent Advances in Learning and Control*, ser. Lecture Notes in Control and Information Sciences, V. Blondel, S. Boyd, and H. Kimura, Eds. Springer-Verlag Limited, 2008, pp. 95–110.

[13] A. Toet, "Image fusion by a ratio of low-pass pyramid," *Pattern Recognition Letters*, vol. 9, no. 4, pp. 245–253, 1989.

[14] A. Toet, L. J. van Ruyven, and J. M. Valeton, "Merging thermal and visual images by a contrast pyramid," *Optical Engineering*, vol. 28, pp. 789 – 792, 1989.

[15] O. Rockinger, "Multiresolution-verfahren zur fusion dynamischer bildfolgen," Ph.D. dissertation, Technische Universitt Berlin, 1999, (in German).

[16] Z. Wang, A. Bovik, H. Sheikh, and E. Simoncelli, "Image quality assessment: From error visibility to structural similarity," *Image Processing, IEEE Transactions on*, vol. 13, no. 4, pp. 600–612, 2004.